ACS APPLIED POLYMER MATERIALS

pubs.acs.org/acsapm

Article

Bioactive Scaffolds Based on Amine-Functionalized Gellan Gum for the Osteogenic Differentiation of Gingival Mesenchymal Stem Cells

Laura Tomasello,[▽] Calogero Fiorica,[▽] Rodolfo Mauceri, Annalisa Martorana, Fabio Salvatore Palumbo, Giovanna Pitarresi, Giuseppe Pizzolanti, Giuseppina Campisi, Carla Giordano, and Gennara Cavallaro*

Cite This: *ACS Appl. Polym. Mater.* 2022, 4, 1805−1815

Read Online

ACCESS | Metrics & More | Article Recommendations | Supporting Information

ABSTRACT: With the aim to produce a cellularized construct for the guided bone regeneration of dento-alveolar defects, here we produce a porous scaffold using an amine derivative of gellan gum to host gingival mesenchymal stem cells (GMSCs) and allow their osteochondral differentiation. Three derivatives were produced by using the same synthetic procedure, and the viscoelastic properties of their aqueous dispersions were investigated and compared to those of the native polysaccharide to choose the derivative with suitable properties for the scaffold production. Freeze-drying was used to obtain a porous sponge that can be rehydrated with the cells' suspension to produce an implantable cell containing hydrogel. We investigated the cytocompatibility of gellan gum-((2-aminoethyl)-carbamate) (named GG-EDA) and the possibility to use it as a starting biomaterial to produce a porous scaffold able to support the osteogenic differentiation of GMSCs. Our data suggest that GG-EDA did not negatively affect the proliferation nor the osteo-inductive capability of the GMSCs.

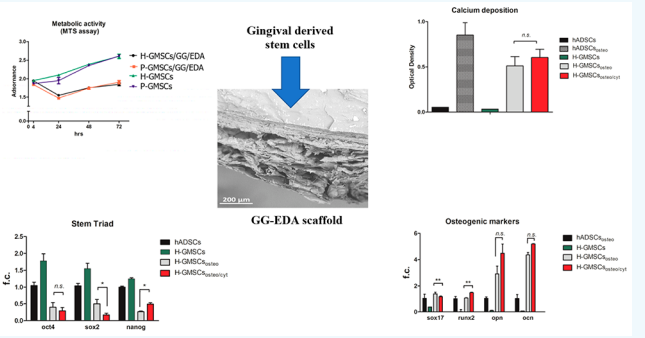

KEYWORDS: *gellan gum, dental bone regeneration, gingival stem cells, hydrogel, osteo-induction*

1. INTRODUCTION

Human adult mesenchymal stem cells (MSCs) are undifferentiated cells distributed in many body districts, with a limited potency related to the stem cell niche in which they are located.[1] MSCs may remain quiescent until they are required to repair a diseased or injured tissue.[2] The knowledge development about MSCs and their hosted environment is based on the new advanced therapeutic strategies, the first being tissue engineering where three-dimensional synthesized matrixes of different biochemical composition are used as scaffolds to culture cells, including endogenous or exogenous MSCs, intended for transplantation.[3,4] In dentistry, in particular, MSC-bioengineered scaffolds have been suggested to improve bone healing and regeneration more like the empty scaffolds or the inoculation of MSCs alone.[5] The guided bone regeneration (GBR), for example, involves the use of biomaterials, which improve repopulation of the defect with osteoprogenitor cells reducing infiltration of the surrounding nonosteogenic tissues.[6−8]

The grafting biomaterial should be able to recapitulate properties of the native extracellular matrix, allowing mechanical support and stimulating osteo-regeneration to provide bone replacement by osteoblast or progenitor cells (i.e., adult stem cells) hosting in the bioactive material (scaffold) itself.

To treat periodontitis, jawbone resorption, and oral defects, several ongoing clinical trials investigate the bone regeneration capability of endogenous gingival mesenchymal stem cells (GMSCs) alone or in combination with collagene, collagene, and hydoxyapatite, synthetic tricalcium phosphate, or absorbed in commercial matrixes. Unfortunately, the efficacy of MSC-based regenerative therapy is not always resolutive, particularly in diseased tissues. In the past decade, GMSCs from discarded diseased gingival tissue have been proposed as a possible cell source for tissue engineering and regenerative therapy.[9] Easy noninvasive procedures needed for their collection and the isolation of a conspicuous number of cells useful for transplantation are ensured.[10,11] Various independent studies confirmed that inflamed tissue-derived GMSCs fully satisfied the minimal criteria proposed by the International Society for Cellular Therapy (ISCT).[12] The inflammatory environment activates cytoskeletal remodeling trough the interaction between several proteins, including chaperone, heat shock proteins, and actin filaments, closely related to the osteogenic

Received: November 17, 2021
Accepted: January 25, 2022
Published: February 4, 2022

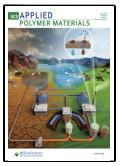

differentiation process.[13] Moreover, cells isolated from waste gingiva retain unaltered stemness properties, including the multilineage differentiation potential, and scaffold adhesion and colonization capability under pro-inflammatory cytokines stimulation.[14−16]

However, the finding of the best bioactive scaffolds for the treatment of dento-alveolar (or dental bone) lesions meets several difficulties, also due to the dynamism of the oral cavity, including the constant presence of saliva that negatively affected its adhesion to the application site. Although synthetic or inorganic biomaterials offer a better mechanical profile, hydrogels provide a natural hydrophilic environment, which allows cell survival and bone growth. Hydrogels can be processed and shaped to the desired geometry, and applied as dry sponges or injected in situ, and can be also easily doped with cells and/or osteoinductive dopants.[17] Numerous studies demonstrated the hydrogels' suitability into mimicking a cellular microenvironment.[18] In particular, polysaccharide-based hydrogels are derived from living tissues, which have macromolecular properties similar to those of the natural extra cellular matrix (ECM).[19] Polysaccharides achieved from algae or plants or from bacterial fermentation have captured the interest of research and industries due to their economic convenience and easy handling.[20] Among the microbial polysaccharides, gellan gum (GG) shows attractive characteristics such as biocompatibility, biodegradability, and tunable gelation conditions and mechanical properties.[21−24] GG and GG blended or composite scaffolds were, for example, successfully employed for bone, cartilage, muscle, and brain tissue engineering as also for antimicrobial or drug delivery applications.[25−28] GG is an anionic tetrasaccharide composed of D-glucose, D-glucuronic acid, D-glucose, and L-rhamnose, produced by *Sphingomonas elodea*. In its native form, GG is acetylated (two acyl groups, *O*-acetate and L-glycerate, are bound to the same glucose residue adjacent to glucuronic acid). The most commercially available GG is the deacetylated form, which produces in water hard, rigid, transparent hydrogels.[29,30] However, native GG suffers some limitations related to poor mechanical and handling properties. In particular, the high temperature (60−90 °C) needed for water dissolution at the relatively high concentration needed for the production of stable physical hydrogels limits the fabrication procedures and suitability for direct cells' encapsulation.[31] Chemical modifications of GG permit one to improve the hydrogels' physical stability and flexibility, handling, and aqueous dispersibility.[32−35] Recently, we proposed an ethylenediamino-functionalized GG derivative, synthesized by using a low molecular weight GG, to obtain a polyampholite hydrogel. The derivative, indicated as GG-EDA, formed hydrogels with improved stability to the hydrolysis and an enhanced elasticity due to the interaction of inserted amino groups with glucuronic moieties of the tetrasaccharide repetitive unit.[36]

Here, we have opted to functionalize high molecular weight GG to retain, along with the peculiar properties conferred by the insertion of pendant amine moieties, all of the physicochemical features of the native polysaccharide. The ethylenediamino derivative of high molecular weight deacetylated gellan was synthesized and characterized to detect how the functionalization affects the viscoelastic properties of the native GG derivative, and then, as a preliminary step to develop a GBR strategy for the treatment of bone dental lesions, the suitability for the adhesion, integration, proliferation, and osteogenic capability of GMSCs to GG-EDA-based hydrogels has been investigated.

2. EXPERIMENTAL PROCEDURES

2.1. Chemicals. Gellan gum (GelzanTM CM), ethylendiamine (EDA), bis(4-nitrophenyl)carbonate (4-NPBC), acetone, 2,4,6-trinitrobenzenesulfonic acid solution (TNBS), anhydrous dimethyl sulfoxide (DMSO), gentamicin, levofloxacin, vancomycin, fluconazole, 3-(4,5-dimethylthiazol-2-yl)-5-(3-carboxymethoxyphenyl)-2-(4-sulfophenyl)-2*H*-tetrazolium (MTS), dexamethasone, β-glycerophosphate, ascorbic acid, acetic acid, and alizarin red were purchased from Sigma-Aldrich (Italy).

Chlorhexidin (Meridol) was supplied by Gaba Vebas S.r.l. (Italy).

Calcein AM and propidium iodide were purchased from Thermo Fisher Scientific (Italy).

Hank's solution (HBSS), fetal bovine serum (FBS), and hydrocortisone were supplied by PAA (Pasching, Austria). Dulbecco's phosphate-buffered saline (DPBS) and Dulbecco's modified Eagle's medium (DMEM)/Ham's F12 medium were purchased from EuroClone (Italy).

Quantitect SYBR Green PCR and the RotorGene Q Instrument were supplied by Qiagen (U.S.). Fibroblast growth factor (b-FGF) and Tumor Necrosis Factor (TNF-α) were purchased from Preprotech (DBA, Italy). Collagenase type II was supplied by Gibco, Life Technologies (Italy). The Rneasy MiniKit was purchased from Qiagen (Italy). Oligo dT primers, $MgCl_2$, and Reverse Transcriptase Rnase were purchased from Improm II, Promega (U.S.). ASC52telo (ATCC SCRC-4000) was from the American Type Culture Collection, U.S.

2.2. Ethics. The protocol was approved by the Internal Ethical Committee of the University Hospital A.U.O.P "P. Giaccone" of Palermo (Internal registry: 5/2014). All subjects gave written informed consent in accordance with the Declaration of Helsinki.

2.3. Synthesis of the Gellan Gum-((2-aminoethyl)-carbamate) (GG-EDA) Derivatives. The synthesis of GG-EDA was performed as previously reported with slight modifications as described in the following.[36] GG was dispersed at 60 °C in DMSO at 1% w/v and kept under magnetic stirring overnight. Subsequently, 4-NPBC, previously dissolved in anhydrous DMSO, was added to obtain a molar ratio between the 4-NPBC and GG repetitive units equal to 0.25, 0.5, and 1, respectively.

After 4 h, a 10-fold molar excess of EDA, with respect to the moles of 4-NPBC, was added, and the reaction was carried out for a further 3 h at 60 °C. The products were isolated by acetone precipitation and then washed several times with the same solvent. Finally, GG-EDA derivatives, named GG-EDA 0.25, GG-EDA 0.5, and GG-EDA 1, were recovered by vacuum-drying at room temperature with a yield, for all of the produced samples, of 90 ± 3% based on the GG initial weight. The derivatization degree in EDA ($DD_{EDA\%}$) of the obtained derivatives was calculated both by ^1H NMR (Bruker Avance II 300 MHz spectrometer) analysis and by the TNBS colorimetric assay. For the NMR analysis, GG or GG-EDA was dissolved at 90 °C in D_2O.

The TNBS assay was conducted as follows. Each derivative was dispersed separately in Milli-Q water at 0.25% w/v. 100 μL of the analyte solution was mixed with 1 mL of TNBS reagent solution (prepared by diluting 50-fold of the stock solution furnished by the supplier with borate buffer pH 9.3), and the resulting solution was incubated for 2 h at 37 °C before its absorbance was analyzed at 500 nm. The analysis was conducted in triplicate. A calibration curve was obtained by analyzing the absorbance at 500 nm of bisPEG-NH_2 aqueous solutions at known concentrations, incubated with the TNBS following the procedure just described for the polysaccharide derivatives. By relating the absorbance at 500 nm obtained for the GG-EDA dispersions with the calibration curve obtained from the standard solutions, it was possible to calculate the degree of functionalization in the ethylenediamine groups of the obtained derivative. The test was also conducted on the GG as a negative control.

https://doi.org/10.1021/acsapm.1c01586
ACS Appl. Polym. Mater. 2022, 4, 1805−1815

2.4. Rheological Measurements of the GG-EDA Derivatives Aqueous Dispersions. Rheological experiments were carried out using a DHR-2 oscillatory rheometer equipped with a self-heating Peltier plate. The geometry used for all of the tests was a cross-hatch parallel plate device with a diameter of 8 mm with a set gap of 300 μm. Hydrogels, obtained by dispersion of GG and derivatives in bidistilled water at 90 °C for 1 h, were tested at 1% and 2% w/v. The obtained samples were kept at 37 °C until use and placed on the lower plate of the rheometer with a spatula before each measurement. Frequency sweep and temperature ramp analysis were performed for GG and GG-EDA 0.25, 0.5, and 1 at both concentrations. In particular, frequency sweep experiments were performed on the hydrogels at 37 °C by applying an increasing angular frequency (from 0.01 to 10 Hz), in the linear viscoelastic region, preliminarily assessed by strain sweep experiments. The spectra were then recorded applying a constant deformation (γ = 5%) in the linear regime. To equilibrate the sample, before each experiment a conditioning sample test was performed by setting a temperature of 37 °C for 60 s and a preshear of 0.1 rad/s for 10 s. To perform thermo-rheological analysis, the samples were exposed to decreasing temperature in the range from 60 to 5 °C, cooling the samples at a rate of 2 °C/min under a constant strain (5%) and angular frequency (0.1 Hz). Samples were previously equilibrated at a temperature of 60 °C for 60 s, and a preshear of 0.1 rad/s for 10 s was performed. To prevent the evaporation of water from the sample, silicon oil was gently poured around the perimeter of the sample. The linear viscoelastic region of the samples was determined at 37 °C with an oscillation strain sweep (0.5−40%) at a constant angular frequency of 0.1 Hz. In addition, for samples at 1.0% w/v, flow ramp measurements were conducted at 37 °C, and shear rates ranging from 0.1 to 1000 s^{-1} were applied for 60 s. All experiments were performed in triplicate, and the average data were used to plot the curves.

2.5. GG-EDA Scaffold Production and Characterization. GG-EDA 0.5 or GG was dispersed in water at a concentration of 5% w/v and at a temperature of 90 °C. The dispersion was kept in the oven until it freely flowed by vial tilting and then left to cool at room temperature to obtain the hydrogel. Samples were frozen at −80 °C and then freeze-dried to obtain the porous scaffold. Scanning electron microscopy (SEM) analysis was conducted using a Phenom XL by Alfatest microscope operating at 5 kV. Differential scanning calorimetry (DSC) and thermogravimetric analysis (TGA) were performed using a DSC/TGA 131 EVO instrument (by SETARAM Instr.).

2.6. Gingival Tissue Extraction and Cell Culture Establishment. Gingival mesenchymal stem cells (GMSCs) were isolated from gingival biopsies of human third molars routinely extracted for orthodontic purposes from six healthy donors (H-GMSCs) aged 46−67 and from molars affected by severe periodontal disease-suffering donors (P-GMSCs) aged 52−78 years. The eligibility criteria for participants were as follows: extraction needed for wisdom teeth for orthodontic reasons or extraction needed for molars suffering from severe periodontal disease (mobility grade III), no suspect or visible pregnancy in females. Only one patient was a current smoker. Before the extraction, each patient performed the oral cavity disinfection protocol rinsing the mouth with 0.2% chlorhexidin for 1 min (Meridol, Gaba Vebas S.r.l., Rome, Italy) to decontaminate the oral cavity. After tooth extraction, gingival tissues were harvested from gingiva flaps during the oral surgery procedures. The gingival tissue was transferred in DMEM:F12 (EuroClone, Milano, Italy) enriched with 0.2 mg/mL gentamicin, 0.25 mg/mL levofluoxacin, 0.10 mg/mL vancomicin, and 0.25 mg/mL fluconazole in a 50 mL tube. Within 24 h, the samples were enzymatically dissociated with collagenase type II (Gibco, Life Technologies, Monza, Italy) for 2 h in a water bath at 37 °C. Isolated GMSCs were placed in 25 cm^2 flasks (p0), kept in IM enriched with 5% fetal bovine serum (FBS) and 20 ng/mL human recombinant basic-FGF (PeproTech, Inc., Hamburg, Germany), and incubated at 37 °C in 5% CO_2. When cultures reached 70−80% of confluence, subculturing at a cellular density of 2 × 104 cells/cm^2 was started (p1). The culture medium was refreshed every 2−3 days, and the antibiotic and antimycotic cover concentration was gradually halved. GMSCs between p1 and p6 were used for the experimental procedures.

2.7. Cell Seeding on Scaffolds. The p3 H-GMSCs or p3 P-GMSCs were seeded on the dry scaffold surface on two different scaffold dimensions (sizes fo 5 × 5 mm for the 96-well and 15.6 × 17.9 mm for the 24-well) placed on 96- and 24-well cell culture plates, respectively (EuroClone, Milano, Italy), at three different cellular densities, 2 × 10^4, 4 × 10^4, and 8 × 10^4 cell/cm^2, in 25 μL by dropping. After a gentle shake, the drop spread into the entire scaffold, a final volume of 100 μL of culture medium was added, and the cells were cultured up to 96 h at 37 °C and 5% CO_2.

2.8. Cell Viability Assay: Evaluation of the Scaffold Cytocompatibility. The cell metabolic activity was evaluated using 3-(4,5-dimethylthiazol-2-yl)-5-(3-carboxymethoxyphenyl)-2-(4-sulfophenyl)-2*H*-tetrazolium (MTS, Sigma-Aldirich) after 4 h of incubation at 37 °C in 5% CO_2. Absorbance was measured at 24, 48, and 72 h in a microplate reader (SpectroStarNano, BMG LABTECH, Ortenberg, Germany) at 490 nm. Measurements were analyzed by Mars Software (BMG LABTECH) and represented as growth curves and a histogram graph on GraphPad Software, Inc., California.

2.9. Cell Visualization on Scaffolds. The cell adhesion capability was evaluated at 1, 2, 3, 4, and 7 days by propidium iodide (PI) and Calcein AM (C-AM) staining according to the Thermo Fisher staining protocol. The fluorescent staining was acquired using a confocal microscope Olympus FV10i at 1, 2, and 3 days and at 1, 4, and 7 days using the fluorescent microscope Leica DMI300. The acquired images were reconstructed with Imagej2 Software.

2.10. In Vitro Bone Formation on Scaffolds. GMSCs were seeded at 4 × 10^4 cell/cm^2, culture or osteogenic differentiation medium (ODM) was added, and the cells were kept for 21 days in the culture. For the ODM, we used Dulbecco's modified Eagle's medium (DMEM) supplemented with 15% FBS, 10^{-4} mM dexamethasone (Sigma-Aldrich), 10 mM β-glycerophosphate (Sigma-Aldrich), and 0.05 mM ascorbic acid (Sigma-Aldrich), with or without 20 ng/mL IL-1β and 40 ng/mL TFN-α. ASC52telo (human adipose mesenchymal stem cells, ATCC SCRC-4000, American Type Culture Collection, U.S.) was used as the positive control.

2.11. Osteogenic Differentiation Analysis. Mineralization of the H-GMSCs with or without 20 ng/mL IL-1β and 40 ng/mL TFN-α was examined by alizarin red S (Sigma-Aldrich, St. Louis, U.S.) staining after 21 days of culture in ODM. After being washed with PBS (Sigma-Aldrich), the samples were fixed in formaldehyde 4%. Alizarin Red staining solution (2%, pH 4.2) was added and incubated in the dark for 30 min. Excess dye was removed by washing with distilled water, and samples were observed under an optical microscope.

For absorbance quantitation, briefly, samples were washed with water, incubated with acetic acid (10% v/v), shaken in a heated plate shaker (Thermomixer C, Eppendorf, Milan, Italy) at 85 °C for 10 min, cooled at 4 °C, and after the samples were transferred in eppendorf tubes, centrifugation was performed. Supernatants were neutralized with ammonium hydroxide, and the absorbance values were detected at 405 nm by a microplate reader (SpectroStarNano, BMG LABTECH, Ortenberg, Germany). Measurements were analyzed by Mars Software (BMG LABTECH) and represented as a histogram graph on GraphPad Software, Inc., California.

2.12. Osteogenesis Marker Detection. The H-GMSCs were seeded into the scaffolds at a density of 4 × 10^4 cells/well and cultured for 21 days in ODM. After differentiation, Osteopontine detection was performed. Briefly, the samples were first fixed with 4% PFA for 15 min at 4 °C, permeabilized with blocking solution added with saponin for 20 min, and kept in a blocking solution (calcium- and magnesium-free PBS plus FBS10%) for 45 min incubated with antihuman osteopontin/OPN/SPP1 primary antibody Alexa Fluor 488 conjugated (AKm2A1, Santacruz) at a dilution of 1:50. After incubation, the samples were observed using the fluorescent microscope Leica DMI300.

https://doi.org/10.1021/acsapm.1c01586
ACS Appl. Polym. Mater. 2022, 4, 1805−1815

2.13. RNA Extraction, Quantification, Reverse Transcription, and Real-Time Quantitative PCR (qRT-PCR). H-GMSCs and P-GMSCs total RNA was extracted and purified using the Rneasy MiniKit (Qiagen, Milan, Italy) according to the manufacturer's instructions. For quantitative and qualitative analysis, Nano Drop 2000 (Thermo Scientific, U.S.) was used. Total RNA reverse-transcription was assessed by the Reverse Transcriptase Rnase kit (Improm II, Promega, U.S.). All qRT-PCR reactions in triplicate were performed via a Quantitect SYBR Green PCR Kit (Qiagen, U.S.) on the RotorGene Q Instrument (Qiagen, U.S.). The reactions were carried out at 95 °C for 3 min of denaturation followed by 95 °C for 20 s, annealing at 60 °C for 30 s, and elongation at 72 °C for 60 s, for 45 cycle repetitions. The specificity of the amplified products was determined by melting peak analysis, and β-actin was used to normalize the expression of the target genes. Gene expression levels were expressed as a fold-change relative to the baseline expression of the target gene in ASC52telo (adipose mesenchymal stem cells, ATCC SCRC-4000, American Type Culture Collection, U.S.) used as a positive cell control according to the e $2^{-\Delta\Delta Ct}$ method ("Analysis of relative gene expression data using real-time quantitative PCR and the 2(-Delta Delta C(T)) Method ("Analysis of relative gene expression data using real-time quantitative PCR and the 2(-Delta Delta C(T)) Method - PubMed", n.d.). All qRT-PCR primers were purchased from Qiagen (QuantiTect Primer Assays, Qiagen, Italy) or Eurofin MWG (Biotech, Bergish Gladbach, Germany) and listed in Table 1. The results were represented as histogram graphs on GraphPad Software, Inc., California.

Table 1. qRT-PCR Primer Sequences

gene	primer sequence/code number	company
actin-β	F: 5′-GGACTT CGA GCA AGA GAT GG-3′	Eurofin
	R: 5′-AGC ACT GTG TTG GCG TAC AG-3′	
nanog	QT0184480	Qiagen
pfn-1	QT00079520	Qiagen
sox17	QT00204099	Qiagen
runx-2	QT00020517	Qiagen
opn	F: 5′-TGT GGG TTT CAG CAC TCT GG-3′	Eurofin
	R: 5′-AAG CGA GTT GAA TGG TGC-3′	
ocn	F: 5′-CTG ACC TCA CAG ATG CCA AG-3′	Eurofin
	R: 5′-GTA GCG CCG GAG TCT GTTC-3	
alp	F: -5′-GCT TCA AAC CGA GAT ACA AG-3′	Eurofin
	R: -5′-CTC GAA GAG ACC CAA TAG GT-3′	

2.14. Statistical Analysis. Each experiment was conducted in triplicate. The data are reported as means ± SD and compared using two-way analysis of variance (ANOVA) with a repetition test. A p-value of less than 0.05 was considered significant.

3. RESULTS AND DISCUSSION

3.1. Synthesis of the Gellan Gum-((2-aminoethyl)-carbamate) (GG-EDA) Derivatives and Rheological Characterization of Aqueous Dispersions. The synthetic route used to functionalize GG with pendant amine moieties, already described in our previous paper[36] to functionalize low molecular weight GG, involves the activation of primary hydroxyl groups of the glucosidic residues of GG with 4-NBPC and the subsequent reaction with a molar excess (with respect to the coupling agent) of EDA. In this work, aiming to produce a hydrogel with a higher hydrolytic resistance and improved stiffness as compared to those already produced from the low molecular weight product, we used unhydrolyzed GG dispersed in DMSO at 60 °C to perform the functionalization with EDA moieties. To demonstrate the reproducibility of the procedure, three derivatives with different theoretical derivatization degrees were produced. The reaction efficiency was investigated by calculating the $DD_{EDA\%}$ for the obtained samples by means of both ^{1}H NMR analysis and TNBS colorimetric assay.

Figure 1 shows the chemical structure and the typical ^{1}H NMR spectrum of the GG-EDA derivatives (in the figure is reported for simplicity only the GG-EDA 0.5 spectrum).

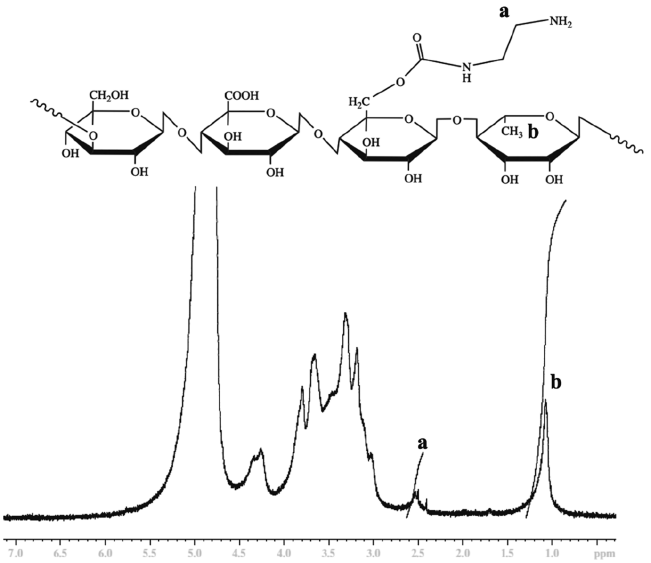

Figure 1. Chemical structure and ^{1}H NMR spectrum of the GG-EDA derivatives (the spectrum is referred to as GG-EDA 0.5). The letters indicate the peaks attributable to the protons of the EDA $-CH_2-$ group vicinal to the free amine group (a) and to the $-CH_3$ protons of GG rhamnose (b).

From the ^{1}H NMR spectrum, the calculation was conducted as reported elsewhere.[36]

As it is possible to notice from the results reported in Table 2, for all of the investigated samples, the $DD_{EDA\%}$ values show no significative differences when calculated with the different analytic assays underlining the reliability of the obtained data.

Table 2. $DD_{EDA\%}$ Values, Calculated by Means of ^{1}H NMR and TNBS Analysis, for the GG-EDA 1, GG-EDA 0.5, and GG-EDA 0.25 Derivatives[a]

sample	$DD_{EDA\%}$ (mol %) ^{1}H NMR	$DD_{EDA\%}$ (mol %) TNBS
GG-EDA 0.25	14.6 ± 1.7	17.1 ± 3.7
GG-EDA 0.5	28.5 ± 2.5	29.4 ± 2.8
GG-EDA 1	49.4 ± 2.6	51.8 ± 3.7

[a]Data are shown as mean ± SEM (n = 6, two independent replicates).

In all of the cases, the reaction efficiency, calculated considering the theoretical molar ratio for the activation of the primary GG hydroxyl groups (moles of 4-NBPC/mol of the GG repetitive unit), is higher than 50%. The sharp standard deviations highlight the reproducibility of the synthetic procedure.

To investigate the effect of the physical interactions between the pendant amino groups and the carboxylic groups of the GG backbone on the viscoelastic properties of the GG-EDA thermo-induced hydrogel, dependent on the $DD_{EDA\%}$, rheological measurements were conducted (Figure 2). In particular, hydrogels were prepared starting with aqueous dispersions at 1% and 2% w/v, and, to evaluate the effect of the

https://doi.org/10.1021/acsapm.1c01586
ACS Appl. Polym. Mater. 2022, 4, 1805−1815

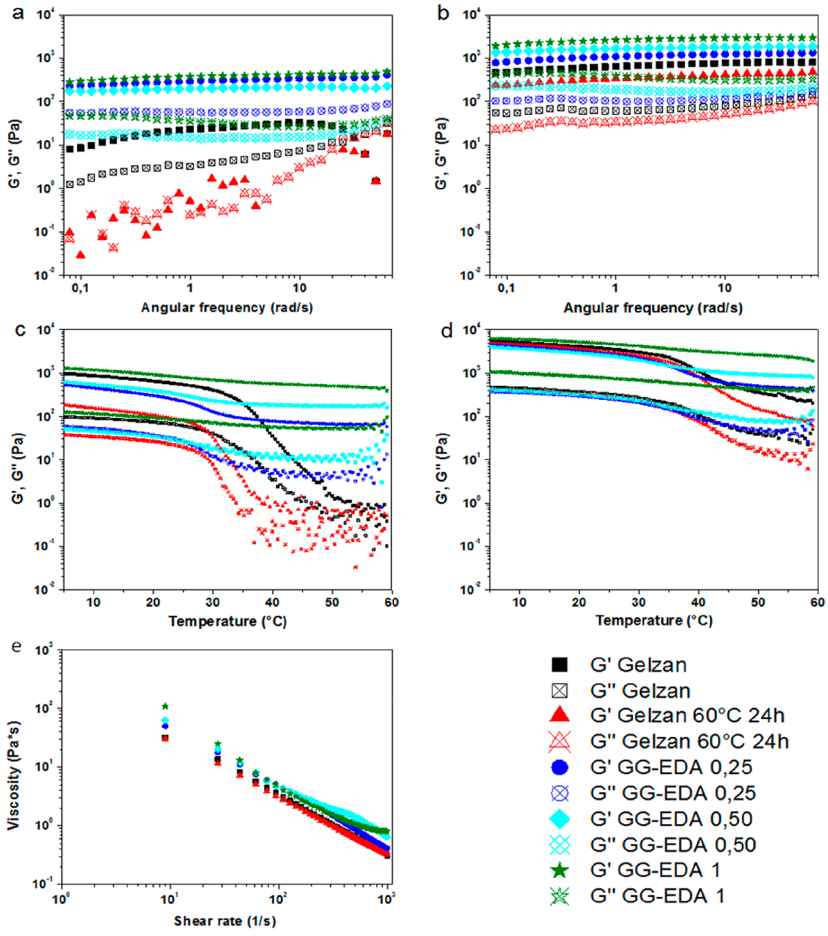

Figure 2. Frequency sweep studies obtained from GG, GG treated at 60 °C for 24 h, and GG-EDA 0.25, 0.5, and 1 at 1% w/v (a) and 2% w/v (b) at a constant strain of 5%; temperature dependence of the storage modulus (G') and loss modulus (G'') of GG, GG treated at 60 °C for 24 h, and GG-EDA 0.25, 0.5, and 1 at 1% w/v (c) and 2% w/v (d) between 5 and 60 °C, at a ramp rate of 2 °C min^{-1}, under a constant strain of 5% and an angular frequency of 0.1 Hz; viscosity values are given as a function of the shear rate of GG, GG treated at 60 °C for 24 h, and GG-EDA 0.25, 0.5, and 1 at 1% w/v (e) at 37 °C.

synthetic procedure conditions on the behavior of the obtained derivatives, for all of the analyses, GG was kept at 60 °C for 24 h was used as the control.

At both concentrations tested, all samples showed a typical gel behavior with a ratio G'/G'' approximately equal to 10 with almost no frequency dependence of the storage (G') and the loss (G'') modulus (Figure 2a,b). The moduli of the gelled hydrogels increase, as expected, as the concentration increases for all samples, and, as compared to GG, the derivatives showed moduli values higher than more than 1 order of magnitude for the 1% w/v samples, confirming the pendant amino moieties strongly affect the physical structure by providing new interactions and reducing repulsion forces between the carboxylic charged groups (Figure 2a). Although the moduli values of the samples at 2% w/v (Figure 2b) showed the same trend, the differences between the derivatives and GG are less significant. Conceivably, as the concentration increases, the interchain repulsion forces become relatively negligible, and the effect of the interactions is less evident.

It is well-known how the temperature often affects the polymers' viscosity, resulting in a decline in the viscosity system. In particular, GG goes through a thermally reversible coil-to-helix transition as the temperature decreases.[37] The thermotropic gelation of GG depends on several factors such as polysaccharide molecular weight and concentration, as well as the presence of cations and the degree of cross-linking.[38]

Interestingly, as $DD_{EDA\%}$ increases, the more considerable is the perturbation on the coil to helix transition, up to an almost totally temperature independence of the moduli in the analyzed range for GG-EDA 0.5 and 1 (Figure 2c). At higher concentrations, the G' values became similar regardless of the derivatization degree. This trend is exacerbated at low temperatures (5 °C) where the G' values become almost the same for all of the investigated samples (Figure 2d).

Considering our previous work results, it can be assumed that the ionic interactions between primary amines and carboxylate groups facilitate the coil to helix transition and stabilize these ordered structures, leading to a higher gelation temperature.

The loss of the thermotropic behavior is important for a scaffold, which has to keep its properties over time without being significantly affected from temperature.

Flow ramp tests were performed for all samples at a concentration of 1% w/v to study the viscosity of the polysaccharides as a function of shear rate. As shown in Figure 2, the viscosity of the GG or GG-EDA derivatives decreases with the increase of sheer rate as a result of the chain alignment to the flow direction. The high share rate makes the interactions between the chains weaker, which resulted in

https://doi.org/10.1021/acsapm.1c01586
ACS Appl. Polym. Mater. 2022, 4, 1805−1815

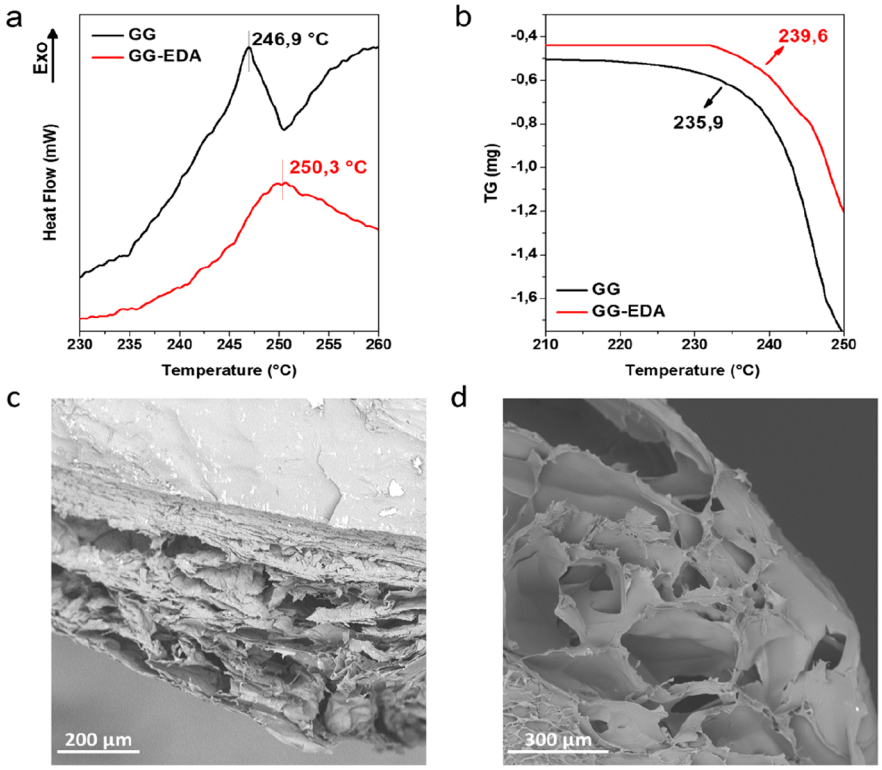

Figure 3. Differential scanning calorimetry (DSC) and thermal gravimetric analysis (TGA) for the GG-EDA 0.5 scaffold as compared to the underivatized GG-based scaffold (a,b): endothermic peak down. Scanning electron microscopy of the cross sections of the GG-EDA 0.5 (c) and GG (d) scaffolds.

the viscosity dropping for all samples with a major effect for the GG that was not functionalized.

3.2. Scaffold Production and Characterization. Rheological analyses corroborated the hypothesis that pendant amine groups, by increasing the number of physical interactions between the GG macromolecules, strengthen and stabilize the hydrated polysaccharide network. It could be than assumed that hydrogel toughness is proportional to the $DD_{EDA\%}$ values. However, it has to be taken into consideration that the functionalization affects also the water dispersibility of the GG-EDA derivatives. In fact, while GG-EDA 1.0 can be hardly dispersed in water at concentrations higher than 3% w/v even at 90 °C, GG-EDA 0.5 and GG-EDA 0.25 produce a clear and fluid dispersion even at 5% w/v at the same temperature. The concentration of the starting macromolecular dispersion plays an important role in producing handling and mechanically stable porous scaffolds. For this reason, taking into consideration the $DD_{EDA\%}$ and the water dispersibility, GG-EDA 0.5 was used to produce the scaffold that, following the hydration, forms the implantable hydrogel. Scaffold was produced by freeze-drying the thermo-induced hydrogel obtained by cooling to room temperature the hot (90 °C) GG-EDA 0.5 aqueous dispersion prepared at 5% w/v. SEM images and DSC/TGA analyses, shown in Figure 3, were conducted to investigate the morphological and physicochemical properties of the sample, respectively, that were compared to those of the unfunctionalized GG scaffold produced in the same conditions.

DSC analysis (Figure 3a) showed that the exothermic peak attributable to the degradation of the polysaccharide passes from 246 °C (native GG) to 250 °C (GG-EDA), while the degradation temperature measured through TGA analysis (Figure 3b) passes from 235 °C (native GG) to 239 °C (GG-EDA). The higher degradation temperature of the GG-EDA 0.5 scaffold as compared to the underivatized GG-based one, shown both by DSC and by TGA analyses, confirms once again the structuring effect of the pendant amine moieties on the hydrogel that corresponds to a higher bulk thermal degradation stability.

The SEM images revealed that, despite the high concentration of the initial dispersions, a porous structure can be obtained through a simple freeze-drying procedure (Figure 3 and d). This aspect is important if one consider that cells have to penetrate into the dried scaffold to be homogeneously distributed into the swollen hydrogel.

3.3. GG/EDA Scaffold Cytocompatibility. Considering the results obtained from the rheologic and physicochemical characterization, in vitro biological assays were conducted using only the GG-EDA 0.5 scaffold.

Cytocompatibility material behavior is the principal prerequisite parameter to be evaluated before medical use. In vitro tests are designed to determine the negative and positive effects that a material imparts on a particular cell type. To investigate the cytocompatibility of the GG-EDA 0.5 hydrogels, G-MSCs or P-GMSCs were seeded on porous scaffolds ($GMSCs_{GG/EDA}$) at three different cell densities (2×10^4, 4×10^4, and 8×10^4 cell/cm^2), and the metabolic activity was investigated using MTS. We found that the GMSCs proliferation was dependent on the cell density used for seeding (data not shown), and the results suggested that the optimal one was 4×10^4 cell/cm^2. Despite this, in $GMSCs_{GG/EDA}$ (test groups), a decrement in the absorbance values at 24 h of culture was detected, both in periodontal and in healthy samples when compared to P-GMSCs and H-

https://doi.org/10.1021/acsapm.1c01586
ACS Appl. Polym. Mater. 2022, 4, 1805−1815

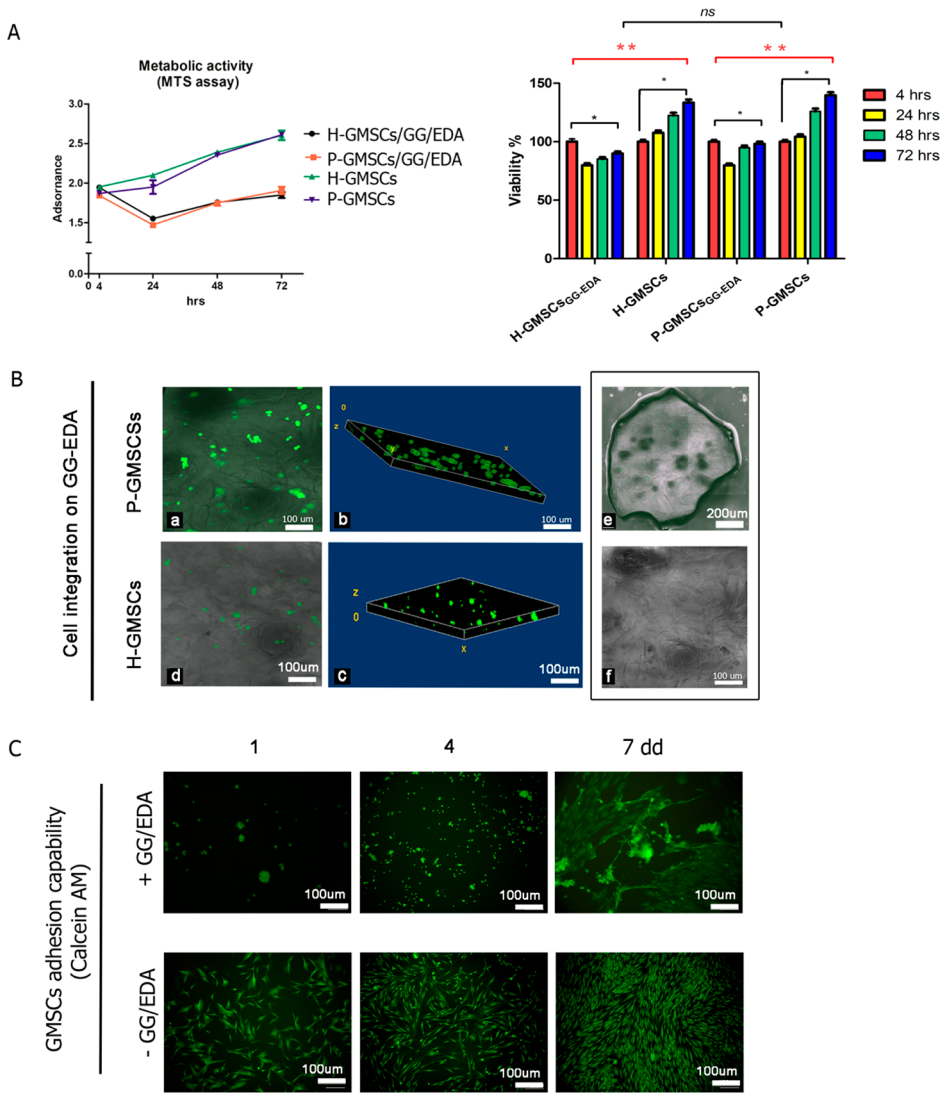

Figure 4. GG/EDA scaffold biocompatibility. (A) MTS assay. In the left panel, the growth curve graph represents the H-GMSCs/GG/EDA (black line), P-GMSCsGG/EDA (red line), H-GMSCs (green line), and P-GMSCs (blue line) growth trend. In the right panel, the histogram graph represents the percentage of viable H-GMSCs/GG/EDA, P-GMSCsGG/EDA, H-GMSCs, and P-GMSCs at 4, 24, 48, and 72 h. *p value > 0.05; **p value > 0.01; ns, p value > 0.05. (B) Cell integration by confocal microscopy. In the left panel is a representative z-stack of images of P-GMSCs (a) and H-GMSCs (d) at 48 h, 40× magnification; a representative volume viewer of P-GMSCs (b) and H-GMSCs (c) at 72 h. In the right panel is a representative image of the cell density distribution map of H-GMSCs on the GG/EDA scaffold placed in a 96-well cell culture plate, at 24 h, 10× magnification (e); GG/EDA scaffold structure and H-GMSCs in brightfield, at 24 h, 40× magnification (f). 100 μm scale bar. (C) Adhesion capability by fluorescent microscopy. Representative images of Calcein AM staining of H-GMSCs on GG/EDA scaffolds (upper panel) and on a 24-well culture plate (lower panel) at 1, 4, and 7 days; 40× magnification, 100 μm scale bar.

GMSCs (controls), suggesting an amount of viable cells corresponding to 77.41 ± 1.55% and 79.82 ± 1.47%, respectively (Figure 4A, histogram graph). The measurements assessed from 24 to 72 h showed a gradual increase in absorbance values, both in P-GMSCs$_{GG/EDA}$ and in H-GMSCs$_{GG/EDA}$, such as to display a comparable growth curve trend with respect to P-GMSCs and H-GMSCs (Figure 4A). No significant difference among the proliferation rate between the test groups and their related controls was detected.

Confocal laser microscopy was used to detect the integration capability of cells on the scaffold. At 48 h by seeding, measure was assessed and z-stacks analysis was conducted: both P-GMSCs and H-GMSCs have been able to colonize GG-EDA scaffolds (Figure 4B-a,d). Data imaged by a z-stacks project appeared as a 2D image, a more intuitive view of cellular distribution from the scaffold surface to the interior part at 72 h confocal analysis was repeated, and measurements were acquired, analyzed, and imaged using a 3D volume viewer on ImageJ2 by the concatenation of all slices acquired (Figure 4B-b,c, P-GMSCs and H-GMSCs, respectively). In Figure 4B1-e,f is given a representative image of a density distribution map analysis of H-GMSCs on GG-ED at 24 h, at 10× magnification and 40× magnification, respectively. It is well-known that material composition and structure can affect the cell shape, and cell spreading is essential for their proliferation. To investigate the capability of the cells to acquire a fibroblast-like phenotype, a fluorescent analysis was conducted for up to 7 days of culture on scaffolds. GG-EDA hindered the H-GMSCs spreading as compared to H-GMSCs cultured on cell culture plastic (Figure 4C). Despite that the H-GMSCs$_{/GG/EDA}$

https://doi.org/10.1021/acsapm.1c01586
ACS Appl. Polym. Mater. 2022, 4, 1805−1815

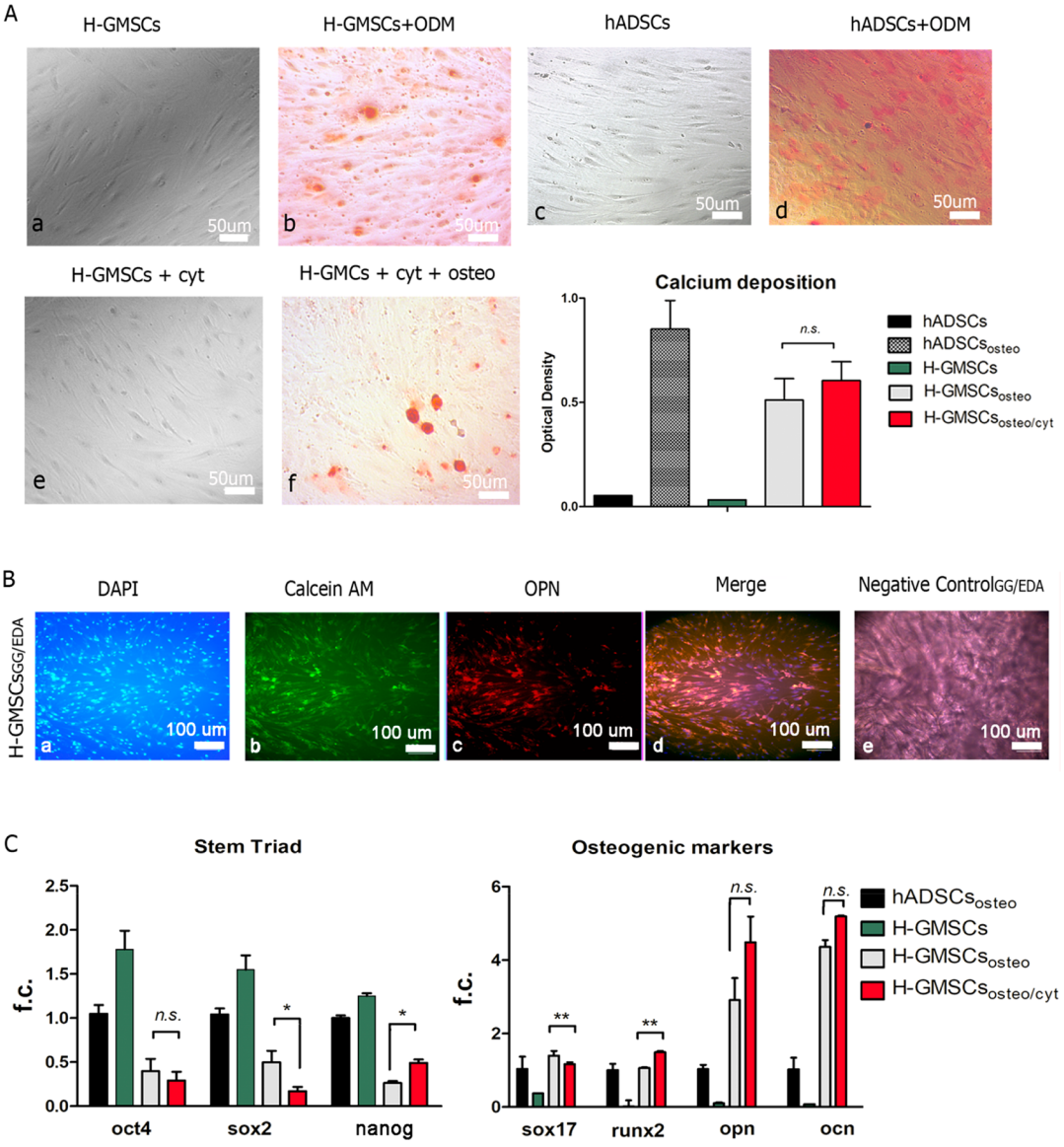

Figure 5. Osteogenic potential of H-GMSCs without or with pro-inflammatory cytokines. (A) Representative image of differentiated H-GMSCs without (b) or with 20 ng/mL IL-1β and 40 ng/mL TFN-α (f) and their relative controls (a,e). hADSC and differentiated hADSCs used as negative and positive controls, respectively (c,d), 20× magnification, 50 μm scale bar. The histogram graph represents the relative quantification of calcium deposition by measure of the optical density of Alizarin Red S. (B) Immunofluorescent analysis of osteopontin protein expression in H-GMSCs/GG/EDA: DAPI blue fluorescence, stained nuclei (a), Calcein AM in green fluorescence, viable cells (b), OPN red fluorescence, stained osteoblast differentiated H-GMSCs (c), merge (d), and empty scaffold (e). 40× magnification, 100 μn scale bar. (C) PCR real-time analysis. The histogram graph represents the mRNA expression levels of specific stem genes oct4, sox2, and nanog (left panel) and of osteogenic-specific genes sox17, runx2, opn, and ocn (right panel) in H-GMSCs with or without pro-inflammatory cytokines and differentiated H-GMSCs with or without pro-inflammatory cytokines. cyt, cytokines; osteo, osteoblast differentiated cells; ODM, osteogenic differentiation medium. *p value > 0.05, **p value > 0.01, ns, p value > 0.05.

retained rounded cells up to 4 days, they preserved their proliferation capacity as shown by the sequence of images in Figure 4C (H-GMSCs/GG/EDA at 1, 4, and 7 days, on upper panel), and at 7 days they have acquired their typical fibroblast-like morphology.

3.4. Osteogenic Differentiation on GG/EDA. To evaluate if GG-EDA affects the GMSC osteogenic differentiation potential, H-GMSCs were seeded on scaffolds and cultivated in ODM for 21 days. Moreover, to reproduce an inflamed environment, IL-1β and TNF-α were added at the ODM along the differentiation culture period. After 21 days, cell cultures were stained with Alizarin Red S, and calcium deposition was detected in each sample (Figure 5Aa-f). To quantify the mineralization rate, the optical density (OD) values of the samples were measured by reading Alizarin Red S at 40 nm using the spectrophotometer's microplate reader (Figure 5A, histogram graph). We found OD values of 0.51 and 0.604 in H-GMSCs plus cytokines and H-GMSCs, respectively. These data suggested mineralization rates of 16.6 and 20.13 s in treated H-GMSCs and H-GMSCs as compared to the undifferentiated control. The detected difference was not significant.

Furthermore, analyses for osteogenic-specific markers were performed. Immunofluorescent analysis detected osteopontin positive expression in H-GMSCs$_{GG/EDA}$ (Figure 5B) at the protein level, and PCR-RT analysis showed the opposite trend

https://doi.org/10.1021/acsapm.1c01586
ACS Appl. Polym. Mater. 2022, 4, 1805−1815

of mRNA level expression of stem-specific genes versus the osteogenic-specific ones (Figure 5C). Specifically, we detected a lower expression of the stem triade, including a down-regulation of oct4 mRNA levels of 0.39-fold and 0.29-fold, of sox2 mRNA levels of 0.49-fold and 0.17-fold, and of nanog mRNA levels of 0.27-fold and 0.49-fold in differentiated H-GMSCs and in differentiated H-GMSCs plus cytokines, respectively (Figure 5C, left panel), whereas a higher expression of osteogenic markers was found. In detail, we found an up-regulation of sox17 mRNA levels of 1.17-fold and 1.39-fold, of runx2 mRNA levels of 1.49-fold and 1.07-fold, of opn mRNA levels of 4.49-fold and 2.91-fold, and of ocn mRNA levels of 5.19-fold and 4.3-fold in differentiated H-GMSCs and in differentiated H-GMSCs plus cytokines, respectively (Figure 5C, right panel).

4. CONCLUSIONS

Amine-functionalized GG derivatives, named GG-EDA, were here produced with three different functionalization degrees in pendant free amine moieties exploiting a reproducible synthetic procedure. Rheological analysis conducted on aqueous solutions of the polysaccharide derivatives reveals that inter- and intramolecular physical interactions occurring between the opposite charged moieties facilitate the typical GG coil to helix transition and stabilize these ordered structures leading to the formation of stiffer hydrogels. The derivative named GG-EDA 0.5 showing optimal features in terms of aqueous dispersibility and viscoelastic properties was chosen to produce a porous sponge through the freeze-drying procedure. DSC and TGA reveal that, as assumed by the rheological analysis, as compared to the unfunctionalized GG, GG-EDA permits the obtainment of a more structured material. In vitro biological studies confirmed that the obtained scaffold was able to support the GMSCs proliferation and osteo-inductive capability and thus can be considered as an optimal candidate for the treatment of bone dental lesions.

■ ASSOCIATED CONTENT

Supporting Information

The Supporting Information is available free of charge at https://pubs.acs.org/doi/10.1021/acsapm.1c01586.

Figure S1: ^{1}H NMR spectrum of GG (PDF)

■ AUTHOR INFORMATION

Corresponding Author

Gennara Cavallaro − *Department of Biological Chemical and Technological Sciences and Technologies (STEBICEF), Laboratory of Biocompatible Polymers, via Archirafi 32, 90123, University of Palermo, Palermo 90133, Italy; Advanced Technology and Network Center (ATeN Center), Università degli Studi di Palermo, Palermo 90133, Italy;* orcid.org/0000-0003-0585-6564; Email: gennara.cavallaro@unipa.it

Authors

Laura Tomasello − *Department of Health Promotion, Mother and Child Care, Internal Medicine and Medical Specialties "G. D'Alessandro" (ProMISE), Laboratory of Regenerative Medicine "Aldo Galluzzo", Piazza delle Cliniche 2, 90127, University of Palermo, Palermo 90133, Italy*

Calogero Fiorica − *Department of Biological Chemical and Technological Sciences and Technologies (STEBICEF), Laboratory of Biocompatible Polymers, via Archirafi 32, 90123, University of Palermo, Palermo 90133, Italy;* orcid.org/0000-0002-5169-4036

Rodolfo Mauceri − *Department of Surgical, Oncological and Oral Sciences (Di.Chir.On.S.), Via Liborio Giuffrè, 590127, University of Palermo, Palermo 90133, Italy; Department of Biomedical and Dental Sciences, Morphological and Functional Images (BIOMORF), University of Messina, Messina 98122, Italy; Department of Dental Surgery, Faculty of Dental Surgery, University of Malta, Msida 2080, Malta*

Annalisa Martorana − *Department of Biological Chemical and Technological Sciences and Technologies (STEBICEF), Laboratory of Biocompatible Polymers, via Archirafi 32, 90123, University of Palermo, Palermo 90133, Italy*

Fabio Salvatore Palumbo − *Department of Biological Chemical and Technological Sciences and Technologies (STEBICEF), Laboratory of Biocompatible Polymers, via Archirafi 32, 90123, University of Palermo, Palermo 90133, Italy*

Giovanna Pitarresi − *Department of Biological Chemical and Technological Sciences and Technologies (STEBICEF), Laboratory of Biocompatible Polymers, via Archirafi 32, 90123, University of Palermo, Palermo 90133, Italy;* orcid.org/0000-0002-0815-9142

Giuseppe Pizzolanti − *Department of Health Promotion, Mother and Child Care, Internal Medicine and Medical Specialties "G. D'Alessandro" (ProMISE), Laboratory of Regenerative Medicine "Aldo Galluzzo", Piazza delle Cliniche 2, 90127, University of Palermo, Palermo 90133, Italy; Advanced Technology and Network Center (ATeN Center), Università degli Studi di Palermo, Palermo 90133, Italy*

Giuseppina Campisi − *Department of Surgical, Oncological and Oral Sciences (Di.Chir.On.S.), Via Liborio Giuffrè, 590127, University of Palermo, Palermo 90133, Italy*

Carla Giordano − *Department of Health Promotion, Mother and Child Care, Internal Medicine and Medical Specialties "G. D'Alessandro" (ProMISE), Laboratory of Regenerative Medicine "Aldo Galluzzo", Piazza delle Cliniche 2, 90127, University of Palermo, Palermo 90133, Italy*

Complete contact information is available at: https://pubs.acs.org/10.1021/acsapm.1c01586

Author Contributions

$^{\nabla}$L.T. and C.F. contributed equally.

Notes

The authors declare no competing financial interest.

■ ACKNOWLEDGMENTS

We are thankful for the valuable contributions of Professor Valeria Vetri, Department of Physics and Chemistry "Emilio Segrè" (Lab Bioimaging and Dosimetria, AteN Center, of the University of Palermo, Italy), for technical support of the confocal microscopy analysis.

■ REFERENCES

(1) Sagaradze, G. D.; Basalova, N. A.; Efimenko, A. Y.; Tkachuk, V. A. Mesenchymal Stromal Cells as Critical Contributors to Tissue Regeneration. *Front. cell Dev. Biol.* **2020**, *8*, 576176.

(2) Mohammad, K.; Dakik, P.; Medkour, Y.; Mitrofanova, D.; Titorenko, V. I. Quiescence Entry, Maintenance, and Exit in Adult Stem Cells. *Int. J. Mol. Sci.* **2019**, *20* (9), 2158.

(3) Choi, Y. C.; Choi, J. S.; Woo, C. H.; Cho, Y. W. Stem Cell Delivery Systems Inspired by Tissue-Specific Niches. *J. Controlled Release* **2014**, *193*, 42−50.
(4) Silva, R.; Fabry, B.; Boccaccini, A. R. Fibrous Protein-Based Hydrogels for Cell Encapsulation. *Biomaterials* **2014**, *35* (25), 6727−6738.
(5) Amghar-Maach, S.; Gay-Escoda, C.; Sánchez-Garcés, M. Á. Regeneration of Periodontal Bone Defects with Dental Pulp Stem Cells Grafting: Systematic Review. *J. Clin. Exp. Dent.* **2019**, *11*, e373−e381.
(6) Murphy, K. G.; Gunsolley, J. C. Guided Tissue Regeneration for the Treatment of Periodontal Intrabony and Furcation Defects.A Systematic Review. *Ann. Periodontol.* **2003**, *8* (1), 266−302.
(7) Elgali, I.; Omar, O.; Dahlin, C.; Thomsen, P. Guided Bone Regeneration: Materials and Biological Mechanisms Revisited. *Eur. J. Oral Sci.* **2017**, *125* (5), 315−337.
(8) Federico, S.; Pitarresi, G.; Palumbo, F. S.; Fiorica, C.; Yang, F.; Giammona, G. Hyaluronan Alkyl Derivatives-Based Electrospun Membranes for Potential Guided Bone Regeneration: Fabrication, Characterization and in Vitro Osteoinductive Properties. *Colloids Surfaces B Biointerfaces* **2021**, *197*, 111438.
(9) Ge, S.; Mrozik, K. M.; Menicanin, D.; Gronthos, S.; Bartold, P. M. Isolation and Characterization of Mesenchymal Stem Cell-like Cells from Healthy and Inflamed Gingival Tissue: Potential Use for Clinical Therapy. *Regen. Med.* **2012**, *7* (6), 819−832.
(10) Tomar, G. B.; Srivastava, R. K.; Gupta, N.; Barhanpurkar, A. P.; Pote, S. T.; Jhaveri, H. M.; Mishra, G. C.; Wani, M. R. Human Gingiva-Derived Mesenchymal Stem Cells Are Superior to Bone Marrow-Derived Mesenchymal Stem Cells for Cell Therapy in Regenerative Medicine. *Biochem. Biophys. Res. Commun.* **2010**, *393* (3), 377−383.
(11) Zhang, Q.; Shi, S.; Liu, Y.; Uyanne, J.; Shi, Y.; Shi, S.; Le, A. D. Mesenchymal Stem Cells Derived from Human Gingiva Are Capable of Immunomodulatory Functions and Ameliorate Inflammation-Related Tissue Destruction in Experimental Colitis. *J. Immunol.* **2009**, *183* (12), 7787−7798.
(12) Dominici, M.; Le Blanc, K.; Mueller, I.; Slaper-Cortenbach, I.; Marini, F.; Krause, D. S.; Deans, R. J.; Keating, A.; Prockop, D. J.; Horwitz, E. M. Minimal Criteria for Defining Multipotent Mesenchymal Stromal Cells. The International Society for Cellular Therapy Position Statement. *Cytotherapy* **2006**, *8* (4), 315−317.
(13) Tomasello, L.; Mauceri, R.; Coppola, A.; Pitrone, M.; Pizzo, G.; Campisi, G.; Pizzolanti, G.; Giordano, C. Mesenchymal Stem Cells Derived from Inflamed Dental Pulpal and Gingival Tissue: A Potential Application for Bone Formation. *Stem Cell Res. Ther.* **2017**, *8* (1), 179.
(14) Tatullo, M.; Codispoti, B.; Pacifici, A.; Palmieri, F.; Marrelli, M.; Pacifici, L.; Paduano, F. Potential Use of Human Periapical Cyst-Mesenchymal Stem Cells (HPCy-MSCs) as a Novel Stem Cell Source for Regenerative Medicine Applications. *Front. Cell Dev. Biol.* **2017**, *5*, 103.
(15) Zhang, F.; Si, M.; Wang, H.; Mekhemar, M. K.; Dörfer, C. E.; Fawzy El-Sayed, K. M. IL-1/TNF- α Inflammatory and Anti-Inflammatory Synchronization Affects Gingival Stem/Progenitor Cells' Regenerative Attributes. *Stem Cells Int.* **2017**, *2017*, 1−9.
(16) Cristaldi, M.; Mauceri, R.; Campisi, G.; Pizzo, G.; Alessandro, R.; Tomasello, L.; Pitrone, M.; Pizzolanti, G.; Giordano, C. Growth and Osteogenic Differentiation of Discarded Gingiva-Derived Mesenchymal Stem Cells on a Commercial Scaffold. *Front. Cell Dev. Biol.* **2020**, *8*, 292.
(17) Bai, X.; Gao, M.; Syed, S.; Zhuang, J.; Xu, X.; Zhang, X.-Q. Bioactive Hydrogels for Bone Regeneration. *Bioact. Mater.* **2018**, *3* (4), 401−417.
(18) Geckil, H.; Xu, F.; Zhang, X.; Moon, S.; Demirci, U. Engineering Hydrogels as Extracellular Matrix Mimics. *Nanomedicine (Lond).* **2010**, *5* (3), 469−484.
(19) Upadhyay, R. K. Role of Biological Scaffolds, Hydro Gels and Stem Cells in Tissue Regeneration Therapy. *Adv. Tissue Eng. Regen. Med. Open Access* **2017**, *2* (1), 121.
(20) Ng, J. Y.; Obuobi, S.; Chua, M. L.; Zhang, C.; Hong, S.; Kumar, Y.; Gokhale, R.; Ee, P. L. R. Biomimicry of Microbial Polysaccharide Hydrogels for Tissue Engineering and Regenerative Medicine − A Review. *Carbohydr. Polym.* **2020**, *241*, 116345.
(21) Oliveira, J. T.; Martins, L.; Picciochi, R.; Malafaya, P. B.; Sousa, R. A.; Neves, N. M.; Mano, J. F.; Reis, R. L. Gellan Gum: A New Biomaterial for Cartilage Tissue Engineering Applications. *J. Biomed. Mater. Res. Part A* **2009**, *9999A* (3), NA-NA.
(22) Bonifacio, M. A.; Cometa, S.; Cochis, A.; Gentile, P.; Ferreira, A. M.; Azzimonti, B.; Procino, G.; Ceci, E.; Rimondini, L.; De Giglio, E. Antibacterial Effectiveness Meets Improved Mechanical Properties: Manuka Honey/Gellan Gum Composite Hydrogels for Cartilage Repair. *Carbohydr. Polym.* **2018**, *198*, 462−472.
(23) Carvalho, C. R.; Wrobel, S.; Meyer, C.; Brandenberger, C.; Cengiz, I. F.; López-Cebral, R.; Silva-Correia, J.; Ronchi, G.; Reis, R. L.; Grothe, C.; Oliveira, J. M.; Haastert-Talini, K. Gellan Gum-Based Luminal Fillers for Peripheral Nerve Regeneration: An *in Vivo* Study in the Rat Sciatic Nerve Repair Model. *Biomater. Sci.* **2018**, *6* (5), 1059−1075.
(24) Coutinho, D. F.; Sant, S. V.; Shin, H.; Oliveira, J. T.; Gomes, M. E.; Neves, N. M.; Khademhosseini, A.; Reis, R. L. Modified Gellan Gum Hydrogels with Tunable Physical and Mechanical Properties. *Biomaterials* **2010**, *31* (29), 7494−7502.
(25) Stevens, L. R.; Gilmore, K. J.; Wallace, G. G.; in het Panhuis, M. Tissue Engineering with Gellan Gum. *Biomater. Sci.* **2016**, *4* (9), 1276−1290.
(26) Kim, W.; Choi, J. H.; Kim, P.; Youn, J.; Song, J. E.; Motta, A.; Migliaresi, C.; Khang, G. Preparation and Evaluation of Gellan Gum Hydrogel Reinforced with Silk Fibers with Enhanced Mechanical and Biological Properties for Cartilage Tissue Engineering. *J. Tissue Eng. Regen. Med.* **2021**, *15* (11), 936−947.
(27) Douglas, T.; Wlodarczyk, M.; Pamula, E.; Declercq, H.; de Mulder, E.; Bucko, M.; Balcaen, L.; Vanhaecke, F.; Cornelissen, R.; Dubruel, P.; Jansen, J.; Leeuwenburgh, S. Enzymatic Mineralization of Gellan Gum Hydrogel for Bone Tissue-Engineering Applications and Its Enhancement by Polydopamine. *J. Tissue Eng. Regen. Med.* **2014**, *8* (11), 906−918.
(28) Douglas, T. E. L.; Dokupil, A.; Reczyńska, K.; Brackman, G.; Krok-Borkowicz, M.; Keppler, J. K.; Božič, M.; Van Der Voort, P.; Pietryga, K.; Samal, S. K.; Balcaen, L.; van den Bulcke, J.; Van Acker, J.; Vanhaecke, F.; Schwarz, K.; Coenye, T.; Pamuła, E. Enrichment of Enzymatically Mineralized Gellan Gum Hydrogels with Phlorotannin-Rich Ecklonia Cava Extract Seanol(®) to Endow Antibacterial Properties and Promote Mineralization. *Biomed. Mater.* **2016**, *11* (4), 045015.
(29) Palumbo, F. S.; Federico, S.; Pitarresi, G.; Fiorica, C.; Giammona, G. Gellan Gum-Based Delivery Systems of Therapeutic Agents and Cells. *Carbohydr. Polym.* **2020**, *229*, 115430.
(30) Kuo, M.-S.; Mort, A. J.; Dell, A. Identification and Location of L-Glycerate, an Unusual Acyl Substituent in Gellan Gum. *Carbohydr. Res.* **1986**, *156*, 173−187.
(31) Bacelar, A. H.; Silva-Correia, J.; Oliveira, J. M.; Reis, R. L. Recent Progress in Gellan Gum Hydrogels Provided by Functionalization Strategies. *J. Mater. Chem. B* **2016**, *4* (37), 6164−6174.
(32) Kirchmajer, D. M.; Steinhoff, B.; Warren, H.; Clark, R.; in het Panhuis, M. Enhanced Gelation Properties of Purified Gellan Gum. *Carbohydr. Res.* **2014**, *388*, 125−129.
(33) Oliveira, J. T.; Santos, T. C.; Martins, L.; Picciochi, R.; Marques, A. P.; Castro, A. G.; Neves, N. M.; Mano, J. F.; Reis, R. L. Gellan Gum Injectable Hydrogels for Cartilage Tissue Engineering Applications: *In Vitro* Studies and Preliminary *In Vivo* Evaluation. *Tissue Eng. Part A* **2010**, *16* (1), 343−353.
(34) Agnello, S.; Gasperini, L.; Mano, J. F.; Pitarresi, G.; Palumbo, F. S.; Reis, R. L.; Giammona, G. Synthesis, Mechanical and Thermal Rheological Properties of New Gellan Gum Derivatives. *Int. J. Biol. Macromol.* **2017**, *98*, 646−653.
(35) Agnello, S.; Palumbo, F. S.; Pitarresi, G.; Fiorica, C.; Giammona, G. Synthesis and Evaluation of Thermo-Rheological

https://doi.org/10.1021/acsapm.1c01586
ACS Appl. Polym. Mater. 2022, 4, 1805−1815

Behaviour and Ionotropic Crosslinking of New Gellan Gum-Alkyl Derivatives. *Carbohydr. Polym.* **2018**, *185*, 73−84.
(36) Fiorica, C.; Pitarresi, G.; Palumbo, F. S.; Mauro, N.; Federico, S.; Giammona, G. Production and Physicochemical Characterization of a New Amine Derivative of Gellan Gum and Rheological Study of Derived Hydrogels. *Carbohydr. Polym.* **2020**, *236*, 116033.
(37) Ogawa, E.; Takahashi, R.; Yajima, H.; Nishinari, K. Effects of Molar Mass on the Coil to Helix Transition of Sodium-Type Gellan Gums in Aqueous Solutions. *Food Hydrocoll.* **2006**, *20* (2−3), 378−385.
(38) Fiorica, C.; Biscari, G.; Palumbo, F. S.; Pitarresi, G.; Martorana, A.; Giammona, G. Physicochemical and Rheological Characterization of Different Low Molecular Weight Gellan Gum Products and Derived Ionotropic Crosslinked Hydrogels. *Gels* **2021**, *7* (2), 62.

https://doi.org/10.1021/acsapm.1c01586
ACS Appl. Polym. Mater. 2022, 4, 1805−1815